POLITECNICO
MILANO 1863

RE.PUBLIC@POLIMI
Research Publications at Politecnico di Milano

Post-Print

This is the accepted version of:

M. Biava, L. Vigevano
Computational Assessment of Wind Tunnel Flow in Closed and Open Section Model Rotor Tests
Journal of the American Helicopter Society, Vol. 59, N. 1, 2014, 012006 (17 pages)
doi:10.4050/JAHS.59.012006

The final publication is available at https://doi.org/10.4050/JAHS.59.012006

Access to the published version may require subscription.

When citing this work, cite the original published paper.

Permanent link to this version
http://hdl.handle.net/11311/787326

Computational Assessment of Wind Tunnel Flow in Closed and Open Section Model Rotor Tests

M. Biava

Senior Aerodynamicist,

AgustaWestland-Politecnico Advanced Rotorcraft Center (AWPARC),

Milano, Italy

L. Vigevano

Associate Professor,

Dipartimento di Ingegneria Aerospaziale - Politecnico di Milano,

Milano, Italy

Abstract

A qualitative analysis of the flow inside the closed and open test sections of the Politecnico di Milano large wind tunnel in presence of rotor effects has been carried out with the *ROSITA* RANS solver. The rotor is represented as an actuator disk. The simulations in the closed section allow for the determination of the flow breakdown boundaries in terms of tunnel operating parameters. In the open section, no flow breakdown may be identified, but the operating conditions in which the rotor wake is escaping from the tunnel circuit can be defined. Some indications are provided on experimental measurements which may be used for an on-line detection of the flow breakdown in the closed section and the wake deflection in the open section.

Nomenclature

C_F force coefficient

Partly presented at the 37th European Rotorcraft Forum, September 13-15 2011

C_P pressure coefficient

C_T thrust coefficient

h rotor height above tunnel floor

R rotor radius

w wind tunnel test section width

x streamwise coordinate axis

y spanwise coordinate axis

z vertical coordinate axis

δ standard deviation

μ advance ratio

σ rotor solidity

Subscript

n normal

x along x-axis

z along z-axis

Introduction

Notwithstanding the increasing capability of CFD methods in predicting rotor performances, the use of wind tunnel test measurements will continue to play a key role in the development of new rotor systems. The question is open, however, on how to operate the model rotor within the wind tunnel so as to reproduce free air conditions. In fact, accurate measurements of rotor performance as achieved in a wind tunnel are strongly influenced by the test section configuration, whether it be closed or open jet.

In closed sections, the wind tunnel walls induce a flow upwash, not uniformly distributed over the rotor disk. Furthermore, at low speed and high rotor thrust conditions, a closed test section may experience what is known as *flow breakdown*, that happens when the interaction between the rotor wake and the tunnel walls strongly modify the flow in the vicinity of the rotor due to the onset of recirculation phenomena [1], [2], [3]. In flow breakdown condition the wind tunnel environment is no longer representative of the free air environment and the rotor performance cannot be adjusted by means of wall corrections, like those proposed by Heyson [4], [5], [6]. Such operating conditions are clearly to be avoided in a test programme. An early attempt to identify the breakdown boundaries in terms of ratio of disk area to wind tunnel cross section area and wake deflection was carried out by Rae [7]. Harris [1] reports breakdown limiting curves in terms of thrust coefficient C_T and advance ratio μ for several rotor dimensions in square section tunnels. Shinoda [8] addressed the study of wall interference effects by means of an extensive experimental campaign in the $80 \times 120\,\mathrm{foot}$ wind tunnel at NASA Ames and identified flow breakdown at $\mu \leq 0.04$ for a thrust range of $0.065 < C_T/\sigma < 0.1$, a somewhat lower limiting μ value than it could be inferred from Harris' results. These experimental findings show the influence of the specific wind tunnel configuration.

In open sections, the corrections required to reproduce free-flight performances are of opposite sign to that of closed test sections. Since the experimental data base for open section rotor tests is small, it is still unclear how to define the flow breakdown regime in these operating conditions. Data reported in [3] seem to show that at low μ values the rotor power gathered in both closed and open sections collapses into a single curve, thus suggesting the occurrence of flow breakdown, but the matter needs to be further investigated.

To this end, a campaign of numerical simulations has been carried out to characterize the flow field generated by the AgustaWestland AW139 model rotor in the closed and open test sections of the Politecnico di Milano (PoliMi) large wind tunnel. The computations were performed with the CFD code *ROSITA* (ROtorcraft Software ITAly), based on the solution of the Reynolds Averaged Navier-Stokes equations coupled with the one-equation turbulence model of Spalart-Allmaras. The rotor effect is represented with an actuator disk model. The numerical solutions were run for several values of the rotor thrust and of the advance ratio. Visualizations of the computed flow field are used to detect the onset of flow breakdown in the closed section and the wake deflection in the open one.

This preliminary investigation represents the first step towards the formulation of wind tunnel corrections, specific for rotor performance tests, by using numerical simulations of the rotor model/wind tunnel system. To partially verify the conclusions of the present work, a limited amount of pressure measurements on the lower deflector of the open test section have been gathered and compared with the numerical results.

The present paper is structured as follows. The numerical methods are briefly described in section 2, while some details on the simulated helicopter rotor, computational grids and flow conditions are given in section 3. The results of the closed section numerical tests are discussed in section 4, where the breakdown boundaries are identified. In section 5 are presented the numerical results for the open section and the comparison with the experimental pressure measurements is reported in section 6. Some conclusions are drawn in the last section.

The flow solver ROSITA

The *ROSITA* CFD solver [9], [10], [11] has been developed at the Aerospace Department of PoliMi over the last ten years, and is currently used and continuously improved at AWPARC. It solves the Euler, Navier-Stokes and Reynolds Averaged Navier-Stokes (RANS) equations in overset systems of moving multi-block grids. The equations are discretized in space by means of a cell-centred finite-volume implementation of the Roe's scheme [12]. Second order accuracy is obtained through the use of MUSCL extrapolation supplemented with a modified version of the Van Albada limiter proposed by Venkatakrishnan [13]. The viscous terms are computed using either a cell-centred discretization scheme, the Swanson and Turkel scheme or the Martinelli scheme. Time advancement is carried out with a dual-time formulation [14]. A 2^{nd} order backward differentiation formula is applied to approximate the time derivative and a fully unfactored implicit scheme is used in pseudo-time. The generalized conjugate gradient (GCG) method is used to solve the resulting linear system, with preconditioning based on a block incomplete lower-upper (BILU) factorization. The RANS equations can be coupled with the simple algebraic models of Michel and Baldwin-Lomax or with the one-equation turbulence model of Spalart-Allmaras.

The connectivity between the component grids is computed by means of the well known Chimera technique. The approach adopted in *ROSITA* is derived from that originally proposed by Chesshire and Henshaw [15]: the domain boundaries with solid wall conditions are firstly identified and all points in overlapping grids that fall close to these boundaries are marked as holes (seed points). Then, an iterative algorithm identifies the donor and fringe points and lets the hole points grow from the seeds until they fill entirely the regions outside the computational domain. To speed up the search of donor points, oct-tree and ADT (alternating digital tree) data structures are employed.

The *ROSITA* solver is fully capable of running in parallel on computing clusters. The parallel algorithm is based on the message passing programming paradigm and the parallelization strategy consists in distributing the grid blocks among the available processors. Each grid block can be automatically subdivided into smaller blocks by the CFD solver to attain an optimal load balancing.

Numerical model and test cases

The numerical details of the simulation are reported for both closed and open test sections.

Closed section

Figure 1 shows the domain used for the simulations of the closed test section of the PoliMi large wind tunnel. The test section is $4\mathrm{m}$ wide and $3.8\mathrm{m}$ high. The grid system consists of a cylindrical mesh, containing the actuator disk representing the AW139 model rotor, and of a background cartesian mesh, modelling the closed test section of the wind tunnel. The actuator disk is placed at a distance $h = 1.9\,\mathrm{m}$ from the floor, that is, in terms of the rotor radius, $h/R = 2.14$, being $R = 0.8875\,\mathrm{m}$. A parameter that is commonly used to correlate the operating conditions to the wall interference effects is the ratio between the rotor diameter and the width w of the wind tunnel test section; for the present case we have $2R/w = 0.44$.

The solution is exchanged between the two grids thanks to the Chimera technique. In total the mesh counts about 2.4 million cells. The background mesh has been created with *ANSYS ICEMCFD*, while the cylindrical mesh has been created with an in-house code. The applied boundary conditions are: inviscid wall boundary conditions on the wind tunnel walls; velocity inlet at the inflow boundary; pressure outlet at the outflow boundary.

The actuator disk is seen as a distribution of linear momentum sources over a disk-shaped grid plane of the cylindrical grid. The distribution of the source strength has been derived by time-accurate

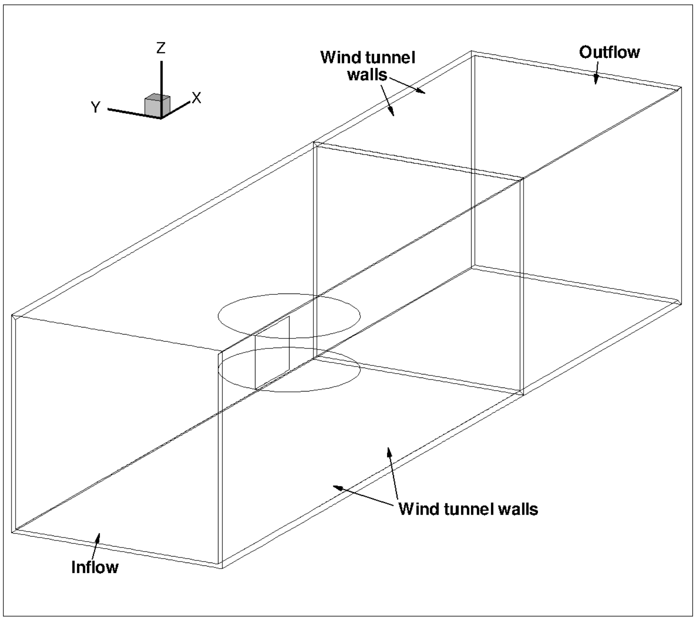

Fig. 1 Boundaries of the closed test section computational grid.

full-rotor forward flight CFD simulations, performed placing the mast in vertical direction and with prescribed rotor kinematics to have zero sine and cosine harmonic components for the flapping motion, so as to maintain the tip path plane parallel to the free stream. The selected configuration can be considered as one which maximize the interference effects between rotor wake and tunnel walls and is very frequently used in model rotor experimental tests for ease of trimming, although may not be the correct one to represent free flight conditions. Consistently, as can be noticed by figure 1, the actuator disk has been positioned parallel to the wind tunnel floor.

The use of a load distribution which does not take into account the actual rotor/tunnel interference conditions and the swirling components of the wake velocities certainly prevent the simulations to obtain quantitative performance corrections. Nevertheless, this simplified wake model is deemed sufficient to characterize the wind tunnel flow during rotor tests, which is the objective of the present investigation.

With respect to the real geometry, the test section grid has the correct dimensions in the cross sections normal to the tunnel axis, but has a higher length downstream of the actuator disk representing the tested rotor. This results in an overall length of the test section grid of $16\mathrm{m}$ instead of the actual $4\mathrm{m}$. The longer downstream region allows the wake to develop and partly dissipate, delaying its interaction with the outflow boundary which could cause the undesired reflection of perturbations inside the flow domain.

The numerical simulations cover the advance ratio interval $0.023 < \mu < 0.21$ for three different value of the thrust coefficient $C_T/\sigma = 0.08, 0.10$, and 0.12. The steady simulations have been performed with the RANS solver using the Spalart-Allmaras turbulence model. The solver was run in parallel on 16 processors so that each test case took about 20 to 40 hours to complete, depending upon the number of iterations needed to attain convergence.

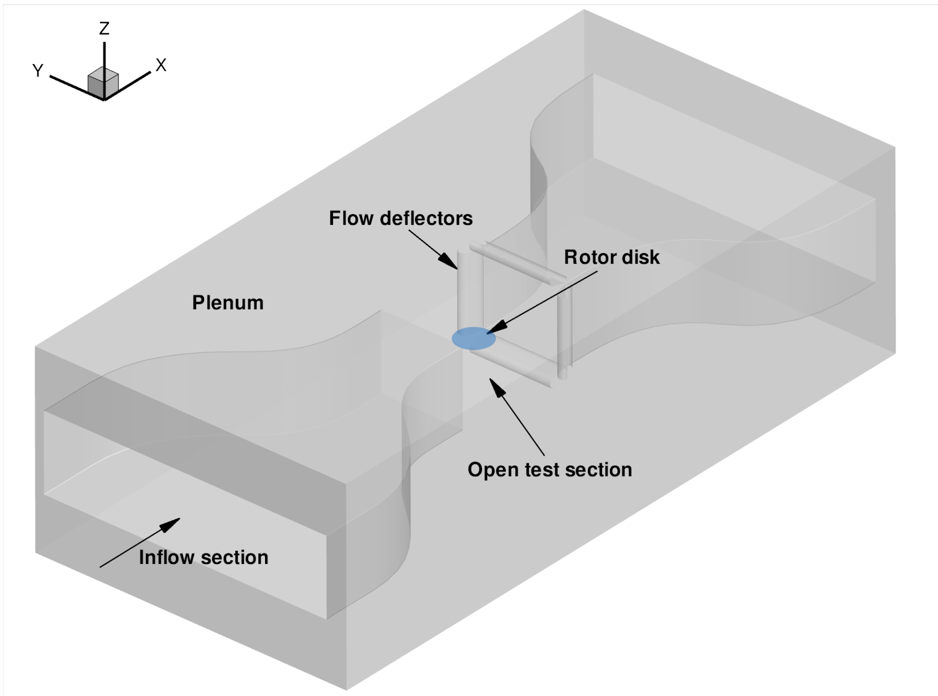

Fig. 2 Numerical domain for the open test section simulations.

Open section

Figure 2 shows the numerical domain used for the simulations of the open test section of the PoliMi large wind tunnel. The Chimera grid system consists in this case of the following components: a background mesh which represents the chamber containing part of the wind tunnel circuit and the open test section. The shape of the wind tunnel and the dimensions of the surrounding chamber were directly taken from a 3D CAD of the wind tunnel; four grids representing the flow deflectors placed at the beginning of the wind tunnel return circuit; a cylindrical mesh for the actuator disk.

The figure 3 reports a slice of the computational mesh in the symmetry plane of the wind tunnel,

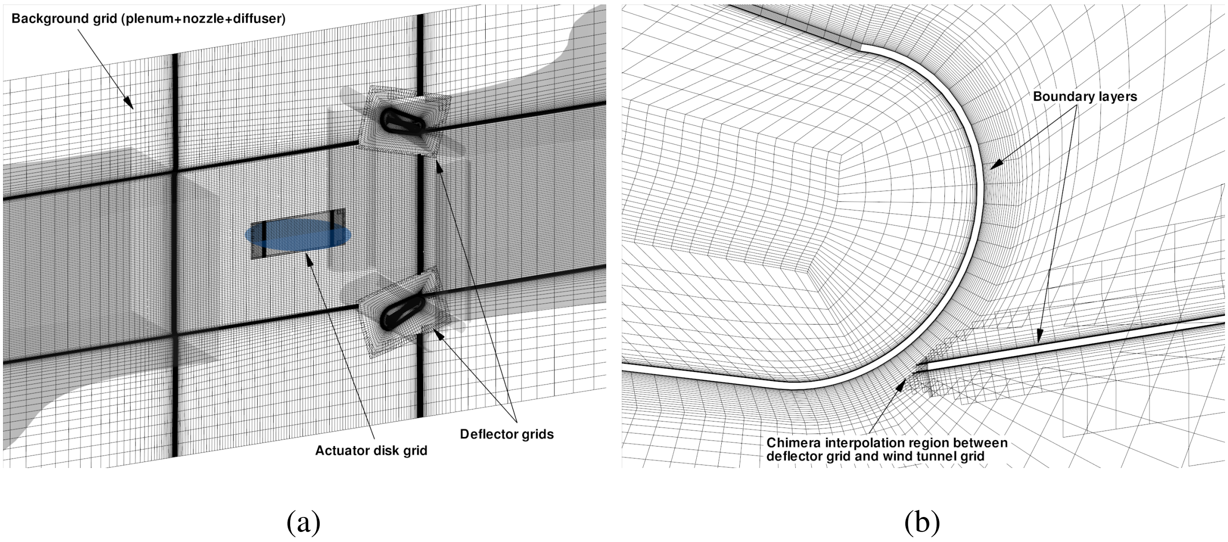

Fig. 3 A slice of the computational grid in the symmetry plane of the wind tunnel (a) and a zoomed view of the slice close to the upper deflector (b).

where the different component grids can be clearly viewed. A magnified view of the mesh close to the upper deflector is also shown in the same figure to make clear the cell distribution in the region of Chimera interpolation between the deflector grid and the wind tunnel grid. It can also be noted that the solid walls (deflectors and wind tunnel walls) have non-zero thickness. In total the mesh contains about 13 million cells. The applied boundary conditions are: viscous wall boundary conditions on the wind tunnel walls; inviscid wall boundary conditions on the chamber walls; velocity inlet boundary conditions at the inflow section; pressure outlet boundary conditions at the outflow section.

The actuator disk model and the range of rotor thrust coefficient values are the same as those used with the closed test section. The considered range of wind tunnel flow speed is limited to the advance ratio interval $0.047 < \mu < 0.163$. The solver was run in parallel on 64 processors so that 26 hours were needed to complete the 5000 iterations at $\mathrm{CFL} = 2.5$ scheduled for each test case.

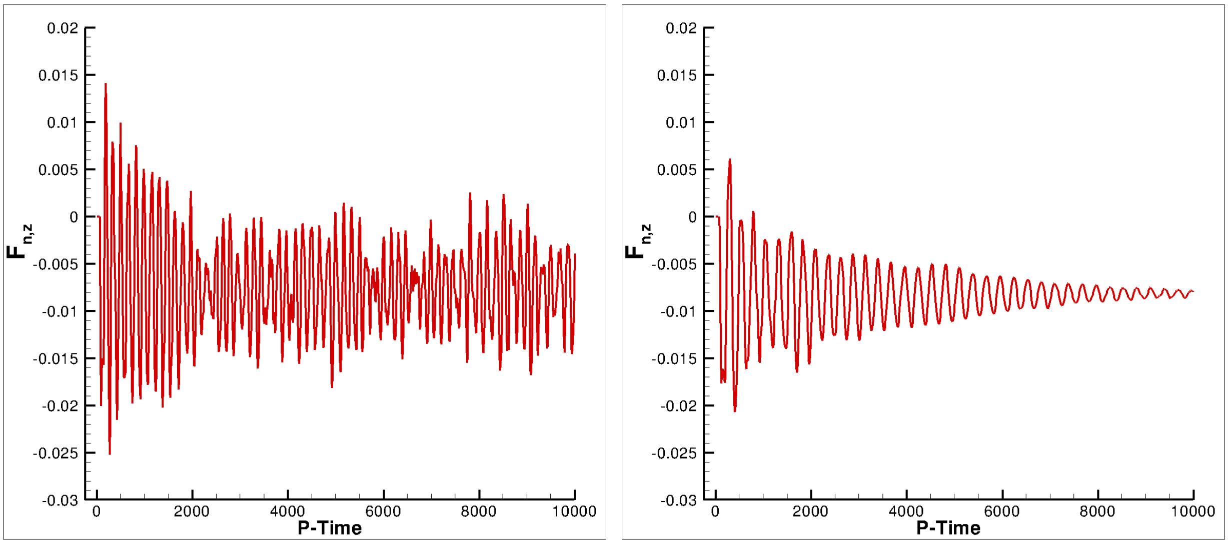

(a) $\mu = 0.023$ (b) $\mu = 0.047$

Fig. 4 Force convergence of the closed section simulations for $C_T/\sigma = 0.10$.

Numerical results for the closed test section

Analysis of results

The analysis is detailed for $C_T/\sigma = 0.10$, while similar conclusions can be drawn for the other considered thrust values.

All the selected wind tunnel and rotor conditions were simulated with the assumption of a steady flow, despite the fact that unsteady phenomena are intuitively to be expected for the flow under investigation. From the analysis of the numerical results we may observe that not all the considered conditions were compatible with a steady flow. Looking at figure 4(a), which shows the force on the wind tunnel floor and normal to it against the number of pseudo-time steps, for the advance ratio $\mu = 0.023$, we notice that the load oscillations are never completely damped out and the solution does not attain a converged steady state. The same happens, to a lesser degree, for advance ratios up to $\mu = 0.047$ (cfr. figure 4(b)). At this low operating speed the rotor wake impinges on the wind tunnel floor and tends to be convected upstream, generating complex (intrinsically unsteady) vortical structures possibly interacting with the rotor itself, as can be observed in figure 5 showing the y-component of the vorticity vector in the vertical symmetry plane of the wind tunnel for $\mu = 0.023 and 0.047$.

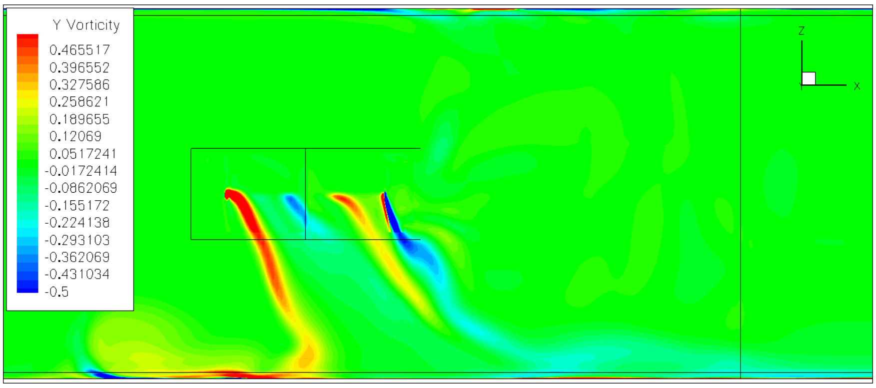

(a) $\mu = 0.023$

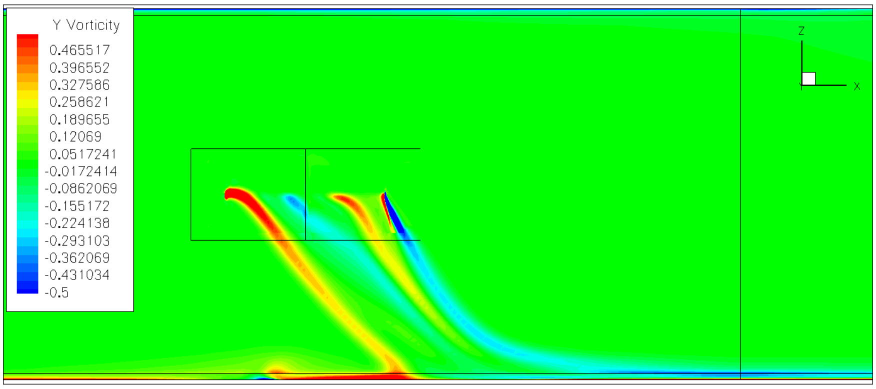

(b) $\mu = 0.047$

Fig. 5 Y-Vorticity in plane $y = 0$ for $C_T/\sigma = 0.10$.

Nevertheless, the (forcedly) steady solutions were retained as a good reference to understand the overall qualitative pattern of the flow inside the wind tunnel test section also at the lower speeds. This is justified in view of the fact that the main objective of the present analysis is to define the boundary of the flow breakdown region. Clearly, the solutions attaining a steady state are characterized by a low level of interaction between the wake and the tunnel walls and are probably representative of free air conditions. *Vice versa*, the solutions that cannot reach the steady state fall in the flow breakdown region, since the unsteadiness is likely to be a symptom of the onset of flow recirculations.

For advance ratios $\mu \geq 0.070$ the simulations seem to reach a reasonably convergent state (see figure 6). For these higher speeds, in fact, there is little or no interaction between the wake and the tunnel walls as can be seen in figure 7, and the flow is thus steady.

Figures 8 and 9 show the local flow Mach number in the cross-flow plane corresponding to the rotor

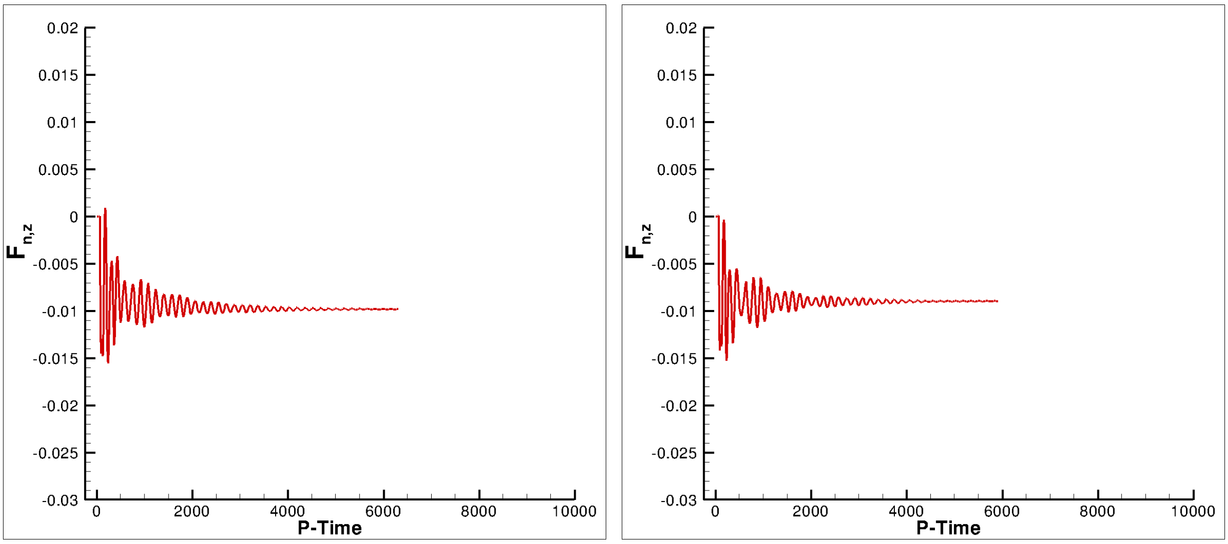

(a) $\mu = 0.070$

(b) $\mu = 0.094$

Fig. 6 Force convergence of the closed section simulations for $C_T/\sigma = 0.10$ at higher advance ratios.

hub and in the symmetry plane of the tunnel, plotted together with the velocity field streamtraces at some selected advance ratios in the range $0.023 < \mu < 0.094$ and with fixed $C_T/\sigma = 0.1$. The solution is taken at the final pseudo-time of the steady calculation.

At $\mu = 0.023$ the pattern of the flow is very complex: the wake of the rotor impinges on the wind tunnel floor right below the rotor itself, then partly moves upstream and generates complex vortical structures with irregular spatial distribution (see figure 8(a)). At this wind tunnel speed, and for all the considered values of the thrust coefficient $C_T/\sigma = 0.08, 0.10, 0.12$, the wind tunnel test is not recommended, due to the strong rotor-wake interaction induced by the wind tunnel walls.

When the advance ratio is raised to 0.047 the flow exhibits a more regular behavior, with the formation of a clearly distinguishable horseshoe vortex close to the test section floor, in front and below the rotor (see figure 8(b)). In this intermediate situation the rotor self-interaction is lower with respect to the $\mu = 0.023$ case, but the deflection of the wake by the tunnel walls is still very strong. This fact and the presence of the horseshoe vortex close to the rotor, make testing in these operating conditions not recommended or, at least, worth for further investigations.

For advance ratios of 0.070 and higher the situation improves significantly (see figures 9(a)–9(b)). At $\mu = 0.070$ the wake impinges on the floor at more than one rotor diameter behind the model, and for

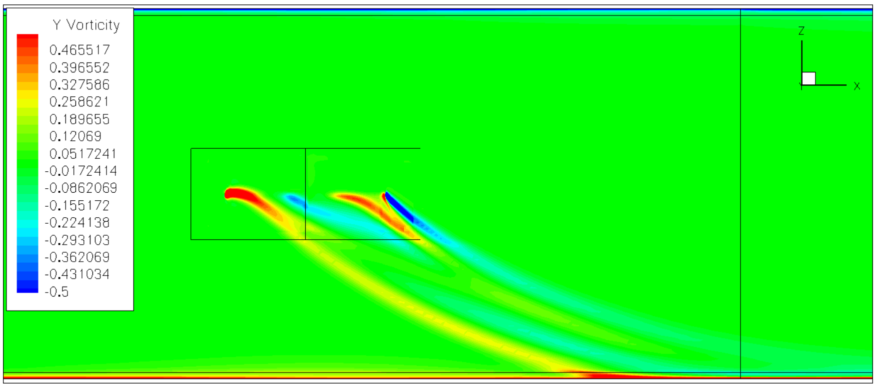

(a) $\mu = 0.070$

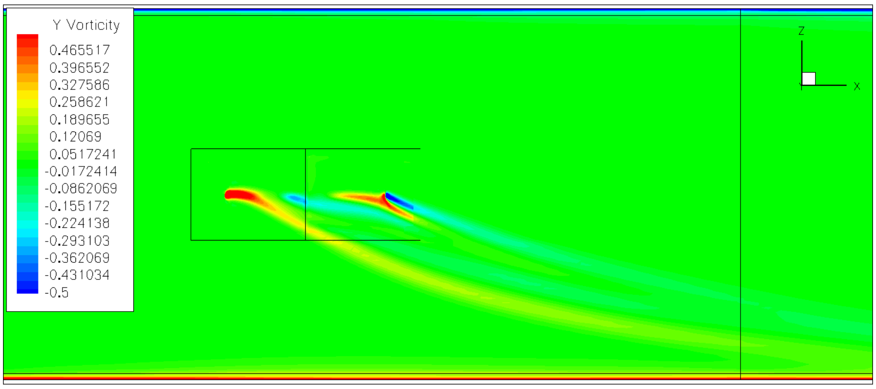

(b) $\mu = 0.094$

Fig. 7 Y-Vorticity in plane $y = 0$ for $C_T/\sigma = 0.10$ at higher advance ratios.

$\mu > 0.094$ there's no more visible strong interaction between the wake and the wind tunnel floor and side walls for at least three rotor diameters. This seems to be compatible with rotor testing and the acquisition of reliable performance data.

Very similar behavior is found for the other considered values of the thrust coefficient, resulting in the same quantitative flow breakdown boundary, $\mu = 0.047$,0.07, which ranges between Shinoda's result [8], $\mu = 0.04$, and the value predicted from Harris' experiments [1]. In fact, for the typical thrust value $C_T = 0.1$ and the $2R/w$ ratio of 0.44, which characterizes the PoliMi wind tunnel, Harris' experimental correlation predicts the breakdown boundary at $\mu \simeq 0.08$, as shown in figure 10.

To sum up, after the analysis of the flow inside the wind tunnel test section for several wind tunnel speeds and rotor thrust coefficients, the following recommendations can be given: regardless of the value of the thrust coefficient in the considered range ($C_T/\sigma = 0.08$,0.12), the wind tunnel environment for

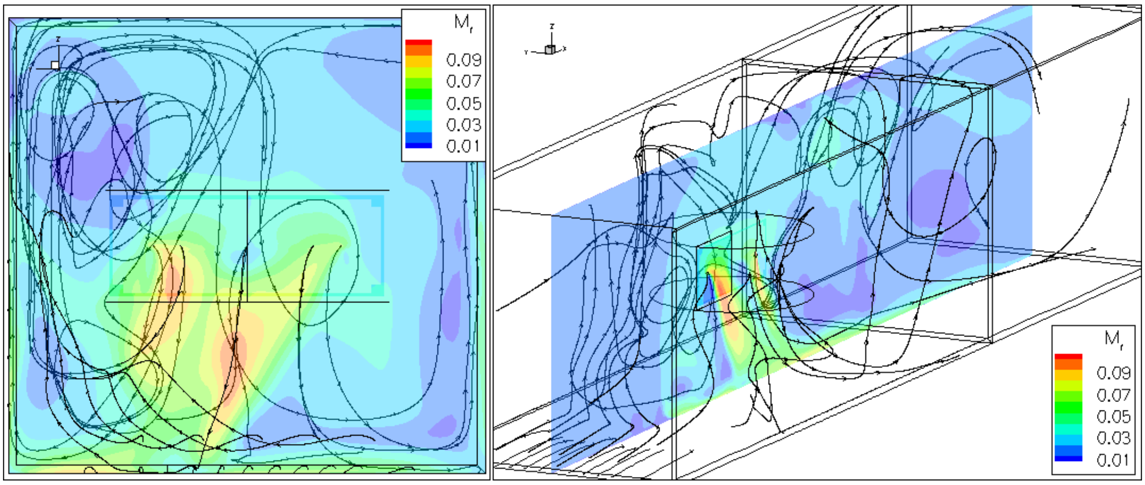

(a) $\mu = 0.023$

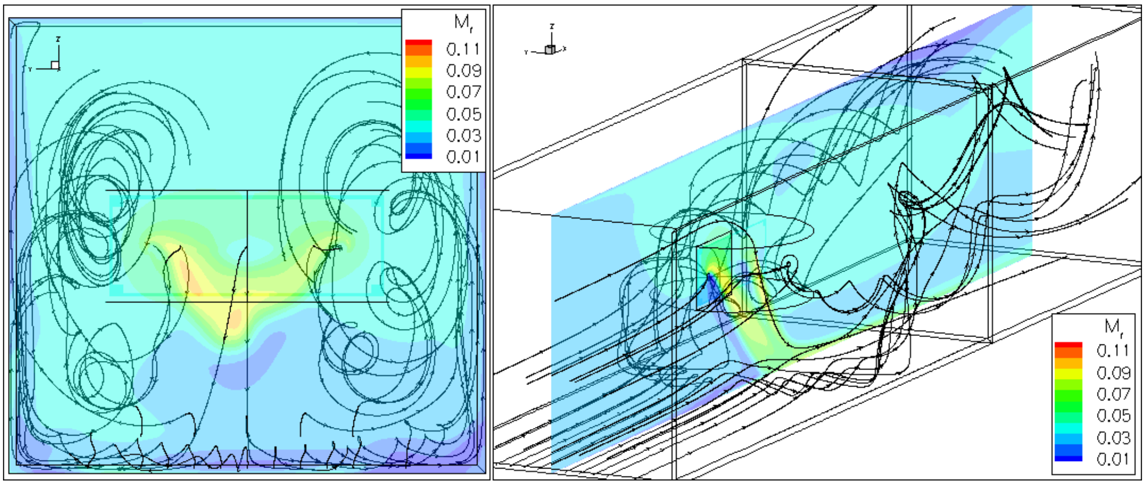

(b) $\mu = 0.047$

Fig. 8 Flow in the closed test section for $C_T/\sigma = 0.10$.

advance ratios higher than 0.070 is representative of free air conditions; for advance ratios below 0.047 the rotor is strongly interacting with its own wake and therefore its performance cannot be corrected to free air by means of a wall correction procedure; the advance ratios in the range 0.047,0.070 represent a transition regime in which the flow breakdown appears, and it is difficult, on the basis of the previous analysis, to tell to what degree the performance measurements can be related to the free air conditions.

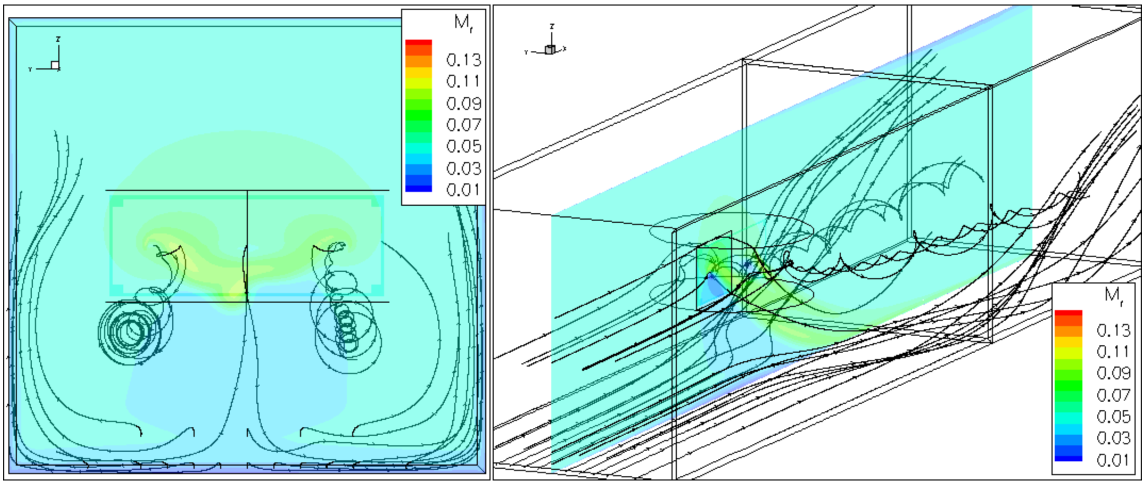

(a) $\mu = 0.070$

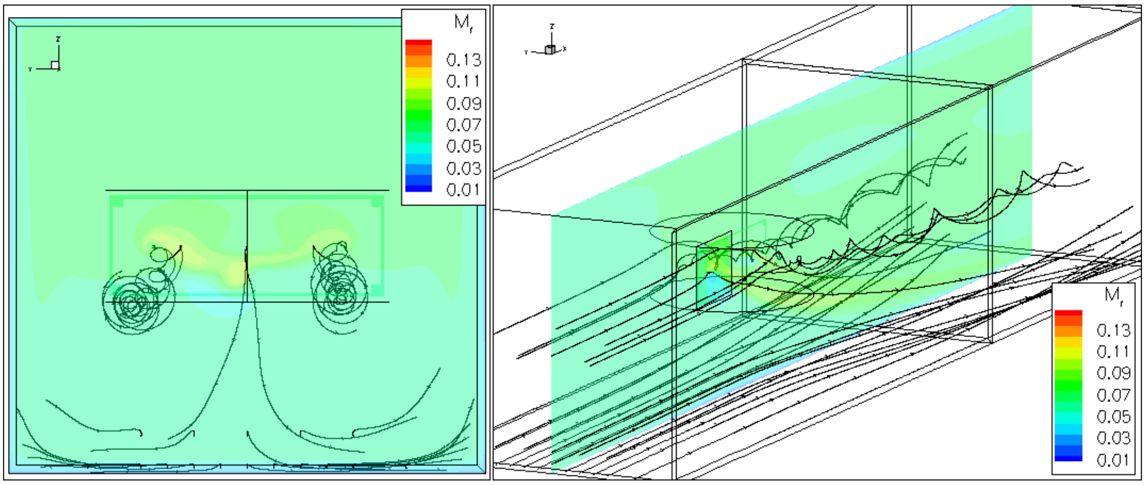

(b) $\mu = 0.094$

Fig. 9 Flow in the closed test section for $C_T/\sigma = 0.10$ at higher advance ratios.

Flow breakdown identification

The analysis of the previous section identified the operating conditions at which flow breakdown occurs in the closed test section of the large wind tunnel of PoliMi. On the basis of the same numerical results, it is possible to give some guidelines on how to detect the flow breakdown during actual wind tunnel tests by monitoring some easily measurable quantities.

Figure 11 presents the pressure distribution on the wind tunnel floor for advance ratios values between 0.023 and 0.094. On the same figure, the streamtraces of the surface shear stress vector field are also plotted.

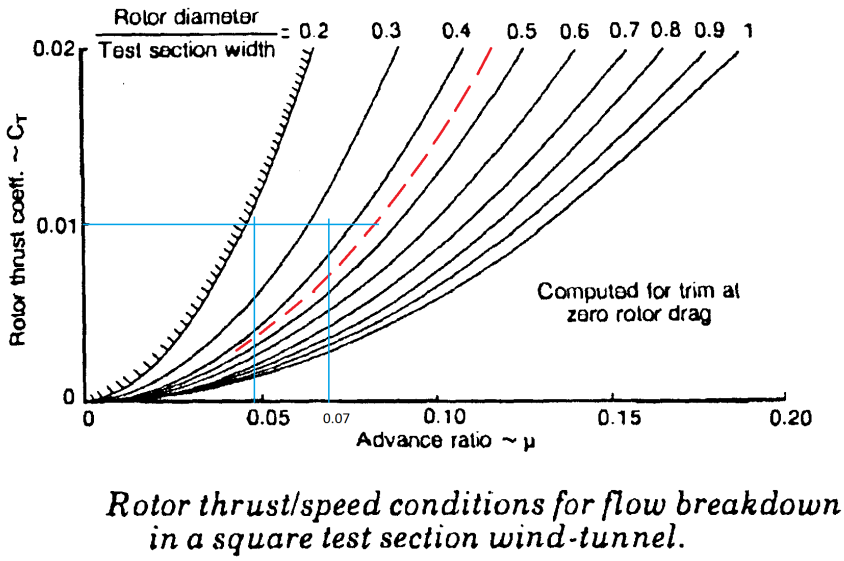

Fig. 10 Flow breakdown boundary curves, from Harris [1]; the dotted curve represents the value $R/w = 0.44$; the vertical lines represent the computed breakdown range for PoliMi wind tunnel.

From the presented results, two possible ways for identifying the occurrence of flow breakdown are suggested. The first one is by measuring the static pressure at some selected points on the centerline of the wind tunnel floor, starting from one diameter in front of the rotor model and down to half/one diameter behind. In fact, it can be noticed that when the downwash impinges on the floor it induces a local raise of the static pressure about the floor centerline. The position of this high pressure spot can in turn be easily related to the flow speed and thus to the onset of the flow breakdown.

However, the measurement of the static pressure could require the drilling of holes on the wind tunnel floor, which may be undesirable. The second, less invasive, option suggested by figure 11 for identifying the presence of flow breakdown is to monitor the shear stress field on the tunnel floor. This can be easily done for instance by sticking lines of wool-tufts on the wind tunnel floor at selected stations in the flow direction, starting from a distance of two diameters ahead of the rotor model and down to half diameter behind.

We deduce that for advance ratios higher than 0.094 all the tufts should direct themselves roughly parallel to the tunnel axis and symmetrically with respect to the vertical symmetry plane of the test section. Additionally, their movements should be very limited to denote the presence of a steady flow.

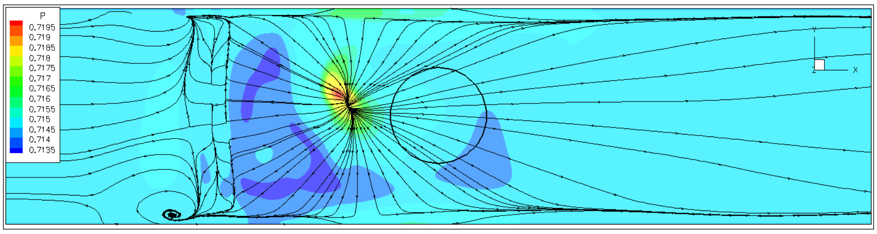

(a) $\mu = 0.023$

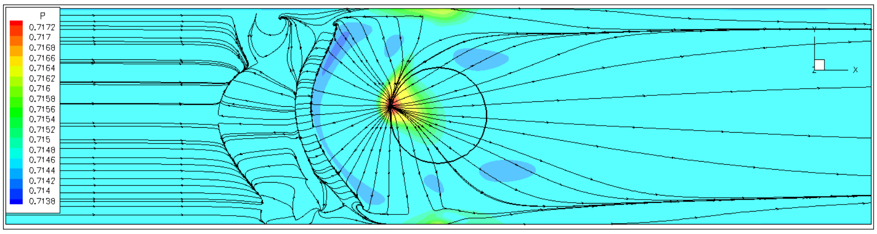

(b) $\mu = 0.047$

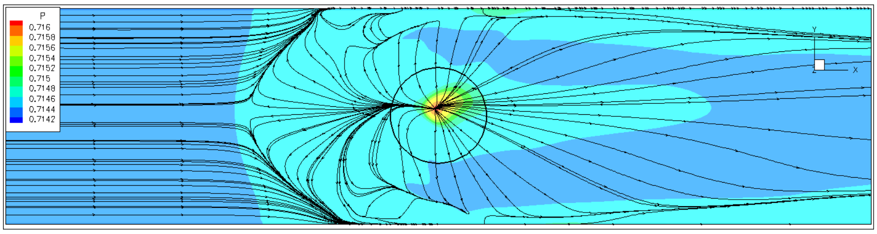

(c) $\mu = 0.059$

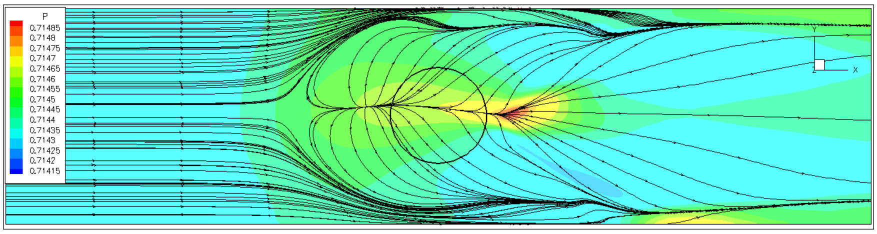

(d) $\mu = 0.070$

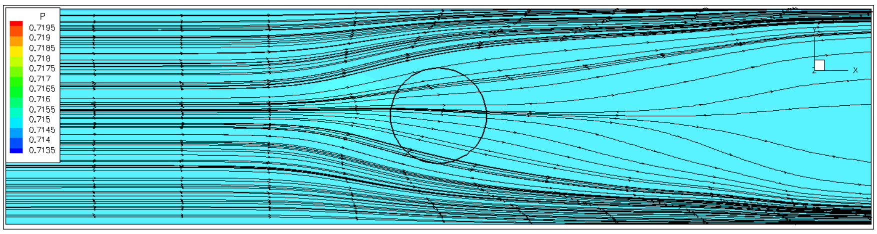

(e) $\mu = 0.094$

Fig. 11 Pressure distribution and streamtraces of the shear stress vector field on the tunnel floor for $C_T/\sigma = 0.10$.

For advance ratios below 0.047, on the other hand, some or all the tufts lines should exhibit a very unsteady movement and the average direction of front lines should be pointing upstream, to reflect the presence of the vortical structures generated by the impingement of the wake on the floor and its upstream motion. Also these flow regimes could therefore be easily detected.

The cases $0.059 < \mu < 0.070$ are in the transition regime and should be characterized by a medium level of unsteadiness of the tufts. Moreover the front lines of tufts should be pointing upstream while the lines below the rotor should be pointing sidewards.

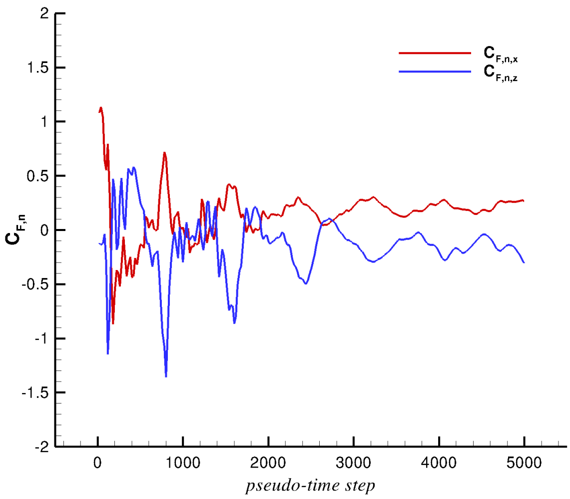

(a) $\mu = 0.047$, $C_T/\sigma = 0.12$

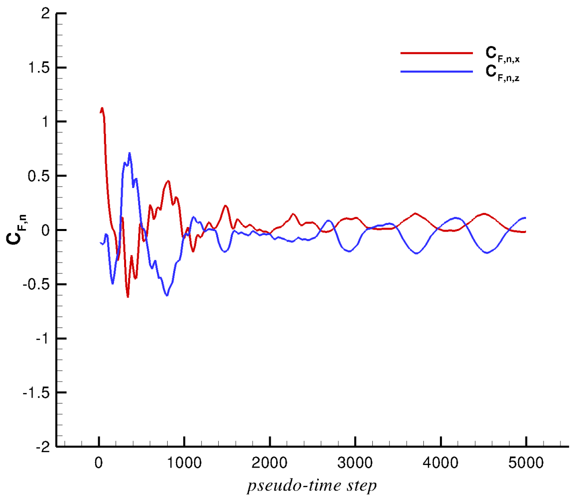

(b) $\mu = 0.163$, $C_T/\sigma = 0.08$

Fig. 12 Force coefficients on the lower flow deflector of the open section.

Numerical results for the open test section

As for the closed section calculations, all the selected test conditions were simulated with the assumption of a steady flow, considering the steady solutions as a good reference to understand the overall qualitative pattern of the flow. Furthermore, for the open section domain an unsteady flow simulation would cost roughly ten times more in terms of computational time. This assumption is deemed reasonable for the goal of the present investigation, being aware that unsteady flow regions are possibly present where the rotor wake impacts on the tunnel walls or on the chamber floor and within the low-speed recirculation zones in the plenum, the latter regions being not relevant in the present work.

Figure 12 shows the convergence of the force coefficients on the lower flow deflector for two opposite operating conditions, that is, respectively, low speed with high disk loading and high speed with low disk loading. $C_{F,n,x}$ and $C_{F,n,z}$ are the aerodynamic force coefficients for the deflector in the x and z directions, respectively. They are based on the flow velocity and density at the outflow section of the wind tunnel nozzle and on the area of the deflector surface projected in the direction normal to its planar inner region. The subscript n indicates that the force coefficients refer only to the integral of the pressure distribution and they do not take into account the tangential stress.

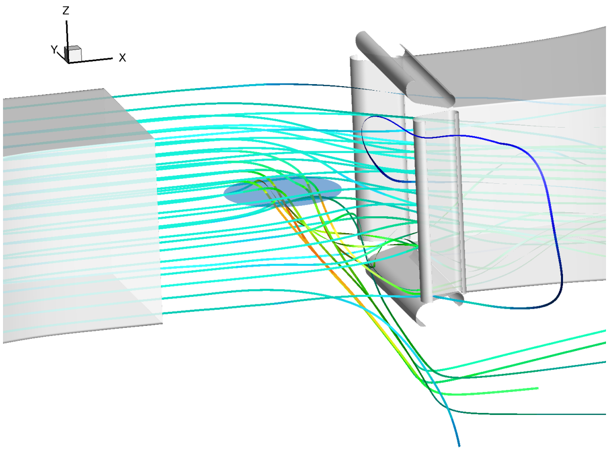

(a) $\mu = 0.047$, $C_T/\sigma = 0.12$

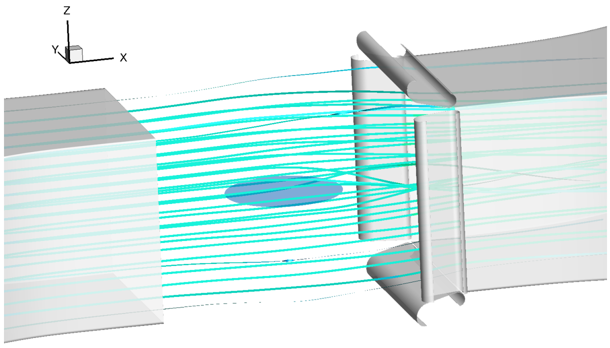

(b) $\mu = 0.163$, $C_T/\sigma = 0.08$

Fig. 13 Streamtraces of the velocity field in the open section.

It is evident that in both cases the solution is not stationary. In particular, at the lower wind tunnel speed, the behavior of the force coefficients is quite irregular and this is reasonably a symptom of a strong interaction between the rotor wake and the wind tunnel walls and flow deflectors. At the higher speed, the variation of the force is more regular (nearly periodic): in this regime the wake/walls interaction is weaker, but the flow is not yet sufficiently stable to reach a steady state.

The above considerations become more clear if we look at figure 13, where the streamtraces of the velocity field are plotted in the region surrounding the open test section of the wind tunnel for the same two operating conditions. At the lower wind tunnel speed and higher disk loading the rotor wake goes downward, partly interacts with the lower flow deflector and then is convected in the chamber right below the return circuit of the wind tunnel, promoting the onset of regions of unsteady, low speed,

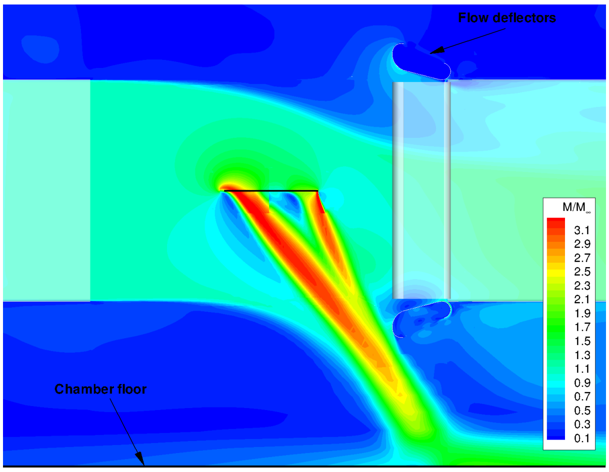

(a) $\mu = 0.047$, $C_T/\sigma = 0.12$

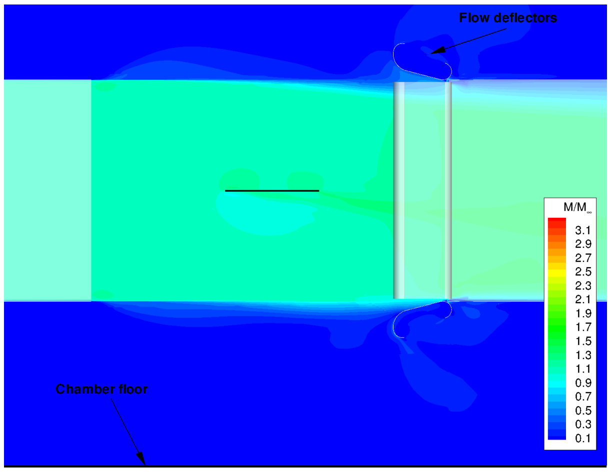

(b) $\mu = 0.163$, $C_T/\sigma = 0.08$

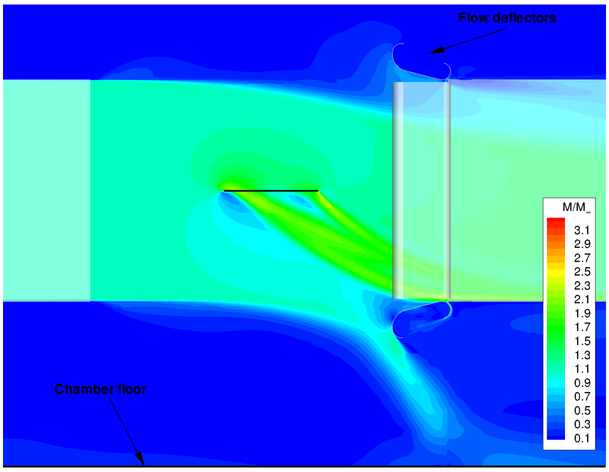

(c) $\mu = 0.07$, $C_T/\sigma = 0.10$

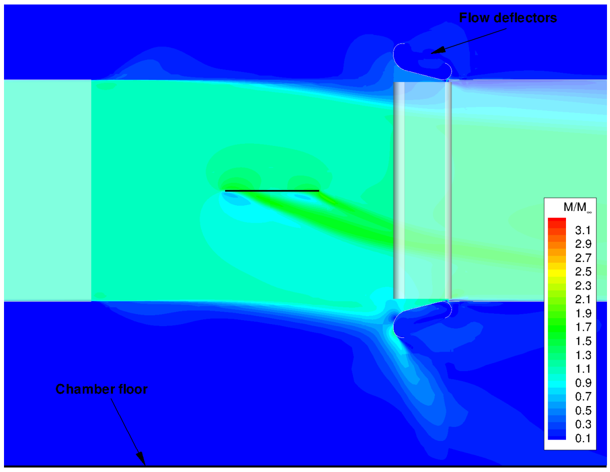

(d) $\mu = 0.117$, $C_T/\sigma = 0.12$

Fig. 14 Mach number distribution in the vertical symmetry plane of the open test section (normalized with respect to the Mach number at the exit of the wind tunnel nozzle).

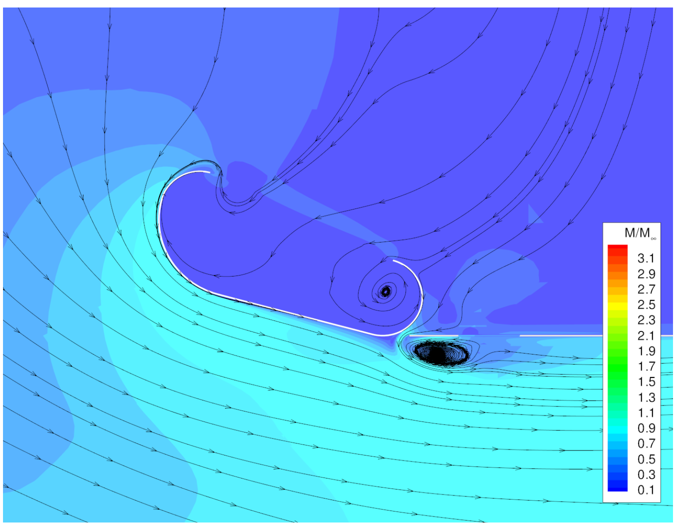

Fig. 15 Mach number distribution in the vertical symmetry plane of the open test section (normalized with respect to the Mach number at the exit of the wind tunnel nozzle): zoom on the region surrounding the upper deflector. $\mu = 0.047$, $C_T/\sigma = 0.12$

recirculating flow. At the higher speed and lower disk loading the wake is instead completely ingested in the return circuit.

The trajectory of the wake for the two operating conditions under analysis is better visualized in figures 14(a)–14(b), showing the normalized Mach number distribution in the vertical symmetry plane of the open test section. The same figures permit to appreciate the effect of the rotor on the wind tunnel nozzle jet. At low wind tunnel speeds the jet is significatively bent downward and, consequently, part of the jet flows outside the wind tunnel circuit and, at the same time, there is a suction of low speed fluid in the upper part of the downstream section of the circuit. It is important to note that the low speed fluid does not interact with the rotor disk, at least in the considered range of wind tunnel speeds, although a strong downwash influences the disk itself. Figure 15 shows the flow in the proximity of the upper deflector, the region where the low speed fluid enters the return circuit of the wind tunnel.

In figures 14(c)–14(d) two other solutions are shown, corresponding to operating conditions laying between the two extreme cases considered so far.

In some of the previously analyzed figures it is possible to note slight discontinuities of the Mach number within the wake of the rotor. They are not actual discontinuities of the flow field, but only plotting artifacts due to the different cell size across the Chimera interface between the actuator disk grid and the wind tunnel grid.

By the analysis of the presented numerical solutions it seems that, for all the considered speeds and rotor thrusts, the flow in the neighborhood of the rotor disk is qualitatively similar to that of the free-flight flow. This conclusion has been checked by comparing the present results with an AD calculation performed in free-flight conditions, for $\mu = 0.047$, $C_T/\sigma = 0.12$. Indeed, from the qualitative visualization of the velocity field and the corresponding streamtraces shown in fig. 16, there is no evident interaction of the rotor with its own wake or with the shear layer of the nozzle jet, even for the considered low value of the advance ratio and high value of disk loading. The only noticeable effect, observed for an intermediate range of velocities and thrust coefficients, is the impact of the wake on the lower deflector, with a possibly consequent ground effect. It is however reasonable to think that the performance measurements gathered in the open test section of the PoliMi wind tunnel might be related to the performance of the real-size rotor in free-flight by a fairly general correction procedure.

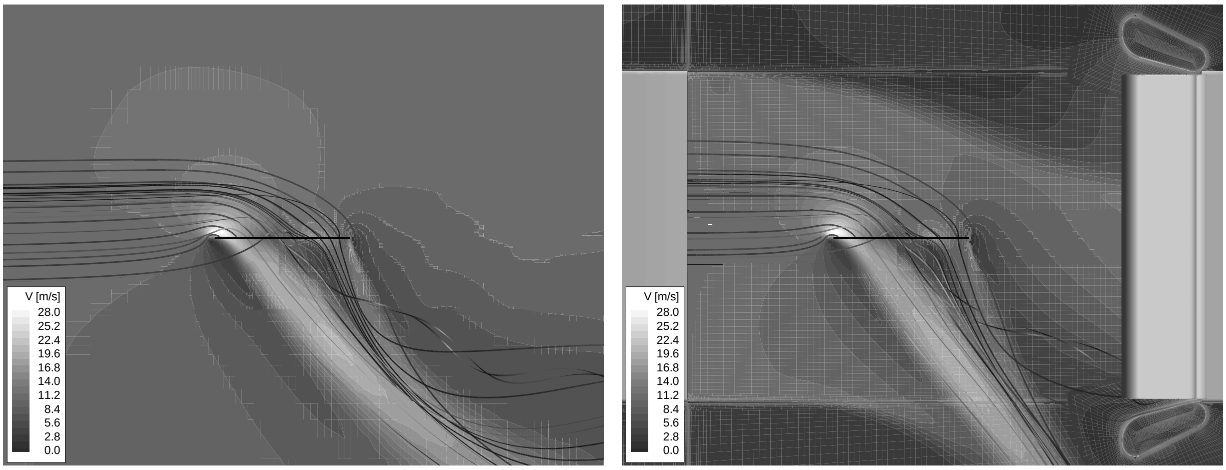

(a) free-flight flow (b) wind-tunnel flow

Fig. 16 Velocity field and streamtraces in the vertical symmetry plane of the rotor for $\mu = 0.047$, $C_T/\sigma = 0.1$.

Nevertheless, there can be other effects that could potentially alter the wind tunnel measurements and need to be investigated. One example of potentially adverse phenomenon is the following: it has been shown that there are operating conditions where part of the wake is ingested by the wind tunnel and part goes outside. In this situation a small perturbation on the wake trajectory alters the energy content of the flow entering the diffuser and thus modifies the dynamics of the wind tunnel circuit. Notwithstanding the high damping characteristics of the tunnel return circuit, the interaction may lead to a perturbation on the jet leaving the nozzle and flowing around the rotor and, in turn, to a modification of the wake trajectory. It is to be verified if the perturbation of the wake trajectory gets damped or if it leads to a limit cycle for some values of the operating parameters. The presented numerical results suggest that this unsteady phenomenon *could* appear for $\mu < 0.117$, but cannot help in predicting if it will be effectively observed or not. A careful monitoring of the wind tunnel state is therefore suggested when operating within the identified critical range.

In order to detect the proximity of such conditions during wind tunnel operation, it is desirable to devise a (simple) means to detect the position of the rotor wake. Pressure probes are among the simplest sensors that can be installed in the wind tunnel and thus we want to rely on pressure measurements in order to estimate the trajectory of the rotor wake. In figures 17 and 18 the pressure coefficient

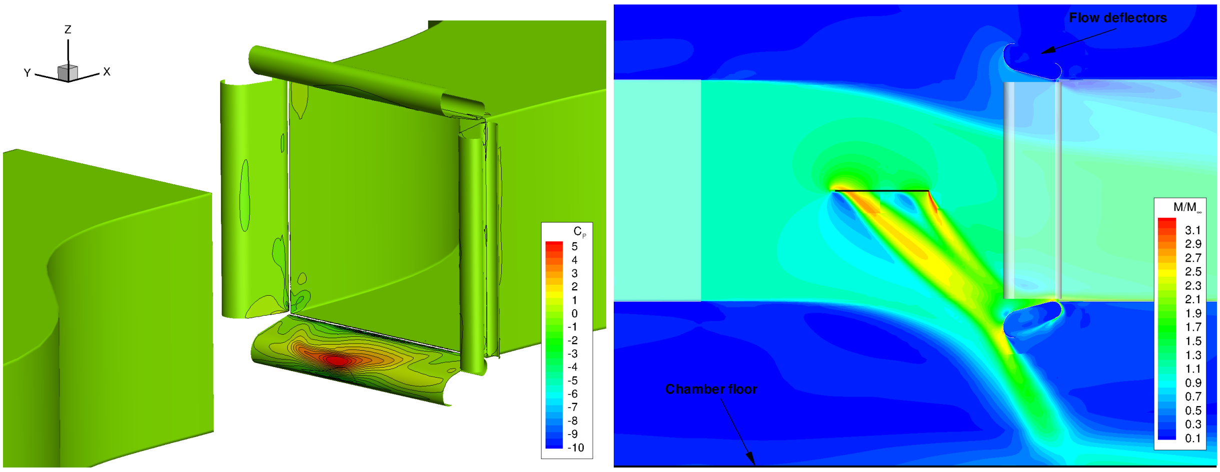

(a) $C_T/\sigma = 0.08$

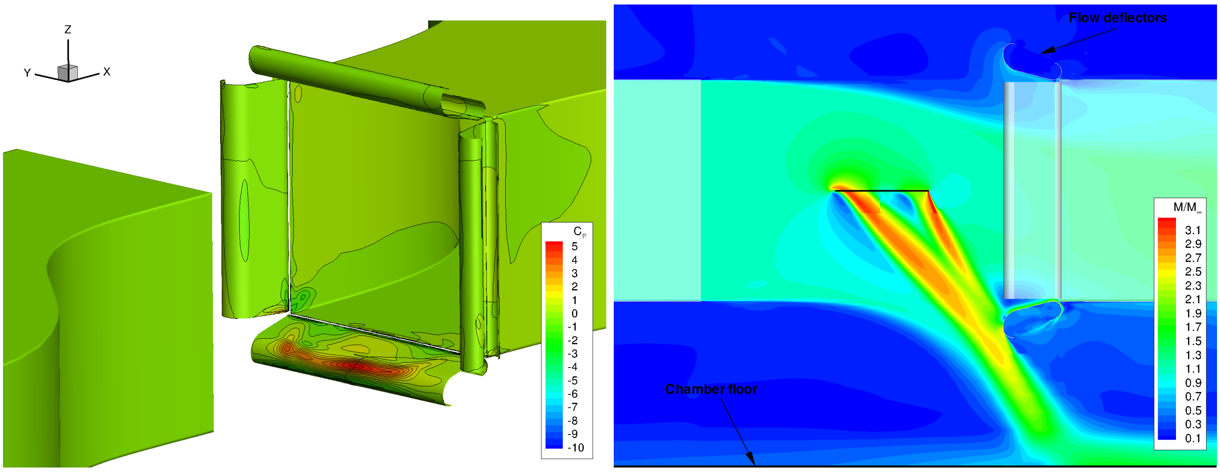

(b) $C_T/\sigma = 0.10$

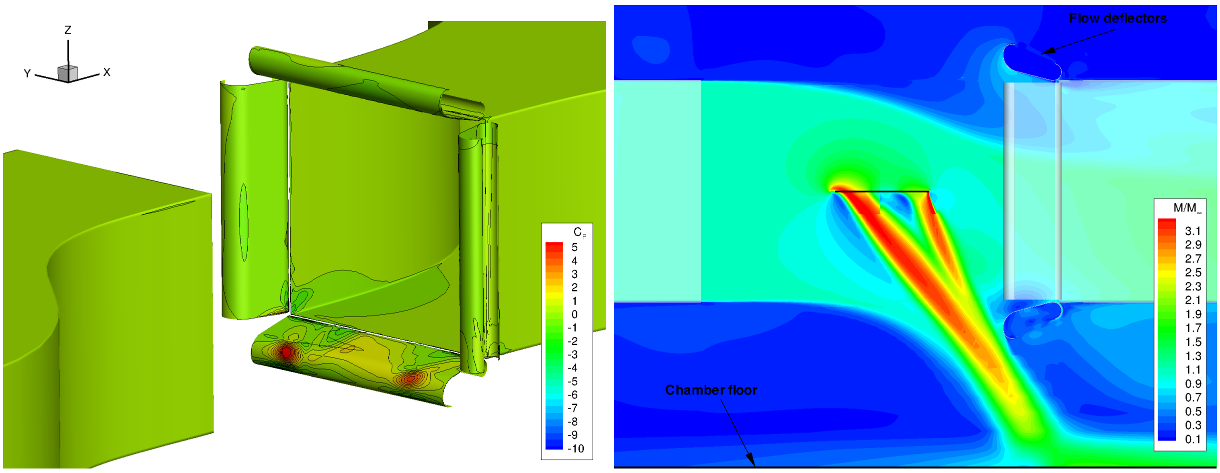

(c) $C_T/\sigma = 0.12$

Fig. 17 Pressure coefficient distribution on the tunnel walls (left) and Mach number distribution in the vertical symmetry plane of the test section (right) for $\mu = 0.047$

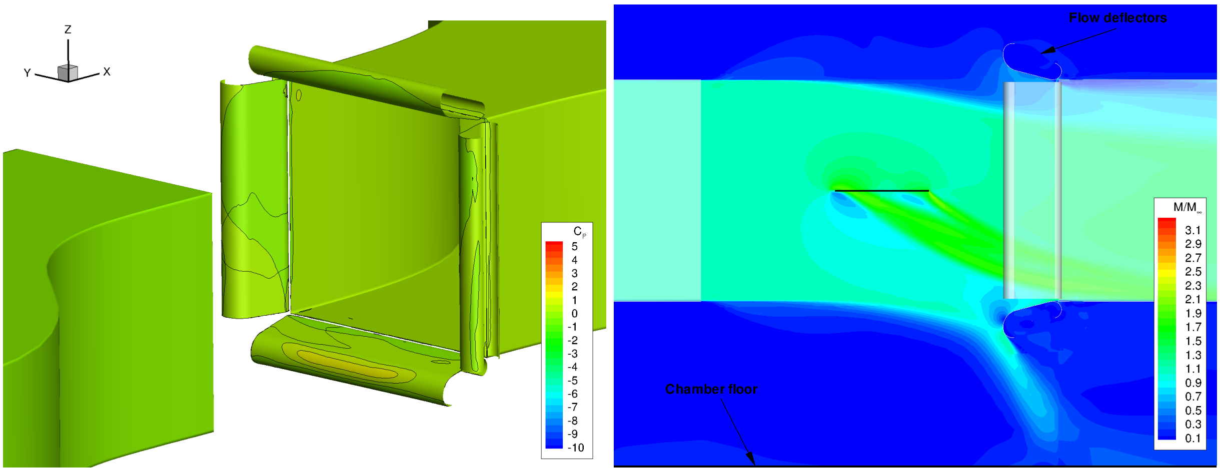

(a) $C_T/\sigma = 0.08$

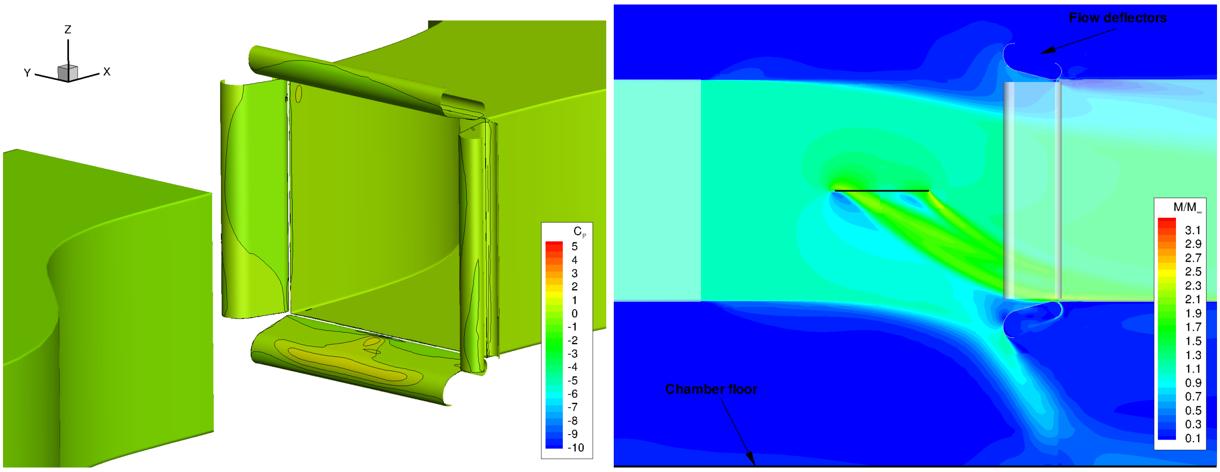

(b) $C_T/\sigma = 0.10$

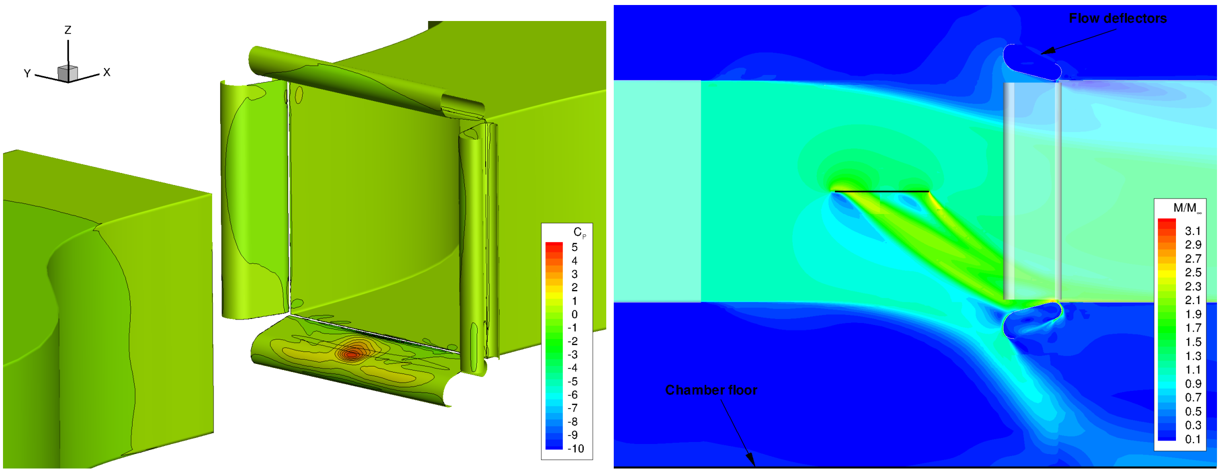

(c) $C_T/\sigma = 0.12$

Fig. 18 Pressure coefficient distribution on the tunnel walls (left) and Mach number distribution in the vertical symmetry plane of the test section (right) for $\mu = 0.070$

distribution on the wind tunnel walls is plotted beside the distribution of the Mach number in the test section vertical symmetry plane for $\mu = 0.047, 0.07$ and for various rotor thrusts. Advance ratios higher than 0.117 are not considered here because at those regimes the wake is completely ingested by the tunnel inlet for all the values of the thrust coefficient. The pressure coefficient is here computed using as reference the pressure and Mach number at the center of the wind tunnel nozzle outlet.

The analysis of the two figures reveals that when the wake is impacting on the lower deflector one or more pressure peaks can be observed on the deflector surface. The distribution of the pressure in terms of the location where the wake impact on the deflector can be summarized as follows.

For $\mu = 0.047$ and $C_T/\sigma = 0.12$ the wake escapes almost completely the wind tunnel inlet but there is no re-ingestion of the wake by the rotor (see figure 17(c)). The effect of the wake impingement on the lower deflector are two symmetric pressure peaks on the leading edge of the deflector, reasonably due to the two main vortices generated by the roll-up of the wake. For lower velocities and higher thrusts it is expected that the wake does not interact any more with the deflector and it is entirely pushed down into the space between the wind tunnel lower wall and the chamber floor.

For the operating conditions between ($\mu = 0.047$, $C_T/\sigma = 0.10$) and ($\mu = 0.07$, $C_T/\sigma = 0.08$), the two pressure peaks coalesce into a single peak located roughly in the middle (in the y direction) of the deflector surface. The peak moves from the leading edge to the trailing edge as the velocity is increased or as the thrust is decreased. In these operating conditions a ground effect due to the interaction between the wake and the deflector could arise.

For $\mu = 0.117$ the wake enters completely the return circuit of the tunnel, and only a slight pressure raise distributed over the leading edge of the lower deflector may be noticed, due to the tunnel jet deflection.

Comparison with measurements for the open test section

From the above description stems that it is possible to monitor the rotor wake position by measuring the pressure at some selected locations on the lower deflector. To this aim, some rows of pressure sensors along the free-stream direction have been installed close to the deflector leading edge at different span

test	μ	C_T/σ
1	0.094	0.10
2	0.070	0.10
3	0.047	0.08
4	0.047	0.12

Table 1. Experimental operating conditions used in the comparison

locations. A limited experimental campaign with the model rotor trimmed with zero flapping angle and horizontal tip path plane has been carried out. The location of the rotor hub during the tests was $0.5\mathrm{m}$ more upstream than that considered in the previous numerical simulations, hence the calculations have been repeated relocating the model rotor within the test section.

The pressure measurements were carried out using a 32 port PSI's ESP-DTC32HD miniature pressure scanner and the pressure signals were acquired by a Pressure Systems' DTC Initium system. For each operating condition, four set of 100 pressure acquisitions were recorded. All four sets were then used to compute the average and standard deviation values.

Experimental data are available for comparison at selected values of the advance ratio and rotor thrust coefficient, as specified in table 1. The comparison of the surface pressure distributions on the lower deflector are shown in figures 19 to 22. The continuous contours represent the numerical results, while the dots represent the experimental data. Note that the pressure scales are different for the different operating conditions, for clarity reasons. In the same figures are also represented the pressure plots along the tunnel symmetry plane; the bar in the graph have a width of twice the standard deviation δ of the measured pressure coefficient.

At the higher considered tunnel velocity, $\mu = 0.094$ ($C_T/\sigma = 0.10$), the wake is entirely laying in the tunnel duct. The open jet is bent downwards by the presence of the rotor and impinges on the low deflector, thus explaining the relatively high value of pressure coefficient, which is not however fully confirmed by the simulations. The calculations predict a symmetrical spanwise pressure distribution, which is quite similar to the experimental data. The maximum value of δ on the centerline in this operating conditions is less than 0.06, which corresponds to 8 $\%$ of the averaged C_P value, indicating a smooth flow on the lower deflector.

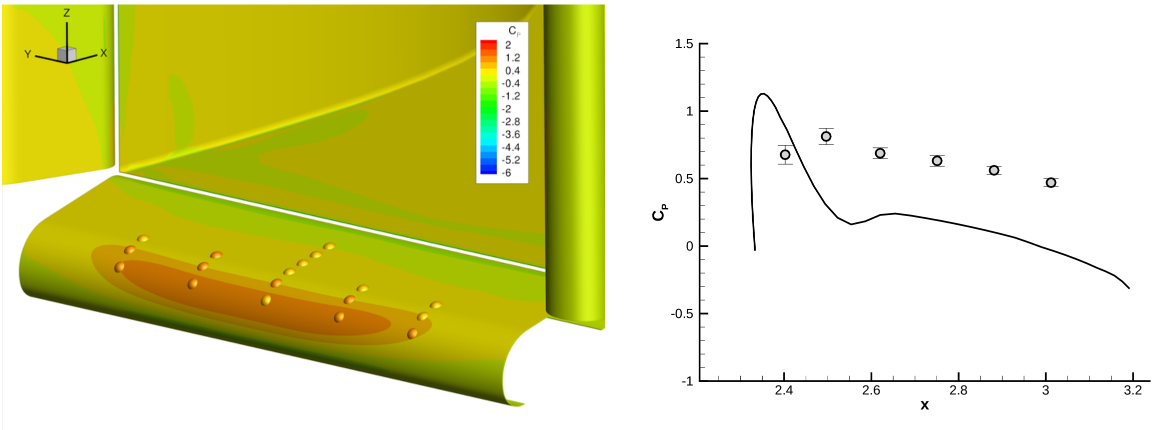

(a) lower deflector (b) symmetry plane

Fig. 19 Pressure coefficient distribution on the lower deflector, $\mu = 0.094$, $C_T/\sigma = 0.1$

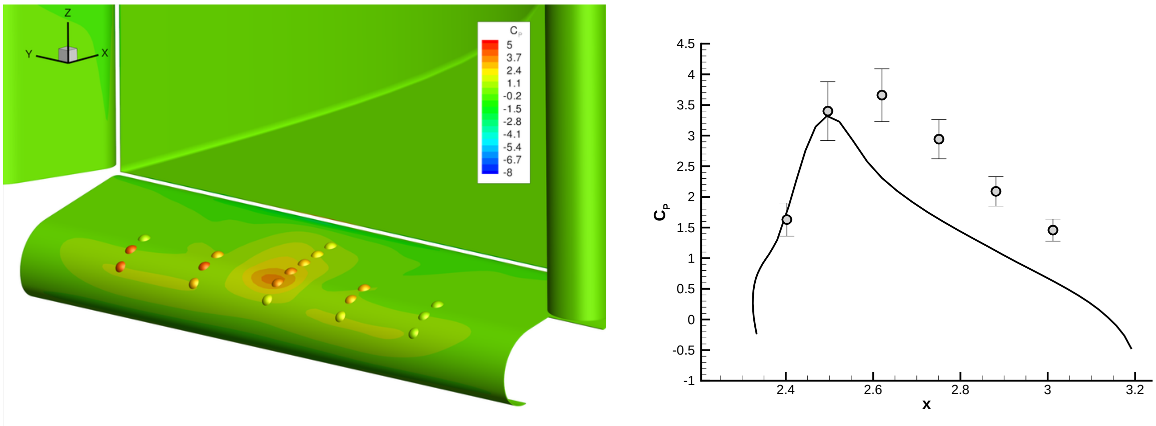

(a) lower deflector (b) symmetry plane

Fig. 20 Pressure coefficient distribution on the lower deflector, $\mu = 0.07$, $C_T/\sigma = 0.1$

When decreasing the tunnel velocity at the same thrust (fig. 20), the wake start interacting with the deflector and the tunnel jet partly escapes from the return circuit. The calculations fail in predicting the asymmetrical experimental distribution. This may be caused by the lack of swirl in the AD computed wake. A relatively good matching of the pressure on the deflector leading edge in the tunnel centerline is observed, although further downstream the level of the measured C_P is significantly higher than the computed one. The maximum value of δ at the centerline increases to 0.48, corresponding to 14 % of the averaged C_P value, indicating the increased unsteadiness of the flow on the lower deflector associated with the wake impingement.

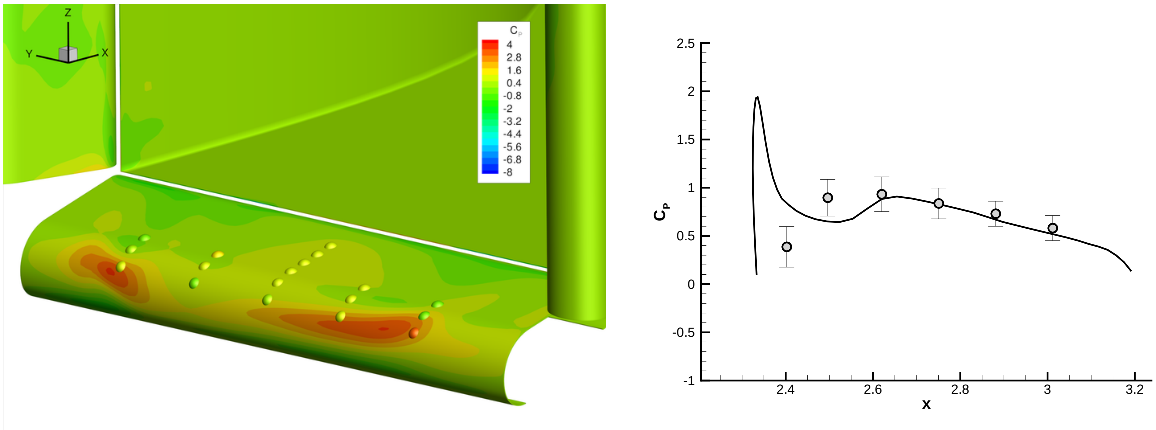

(a) lower deflector (b) symmetry plane

Fig. 21 Pressure coefficient distribution on the lower deflector, $\mu = 0.047$, $C_T/\sigma = 0.08$

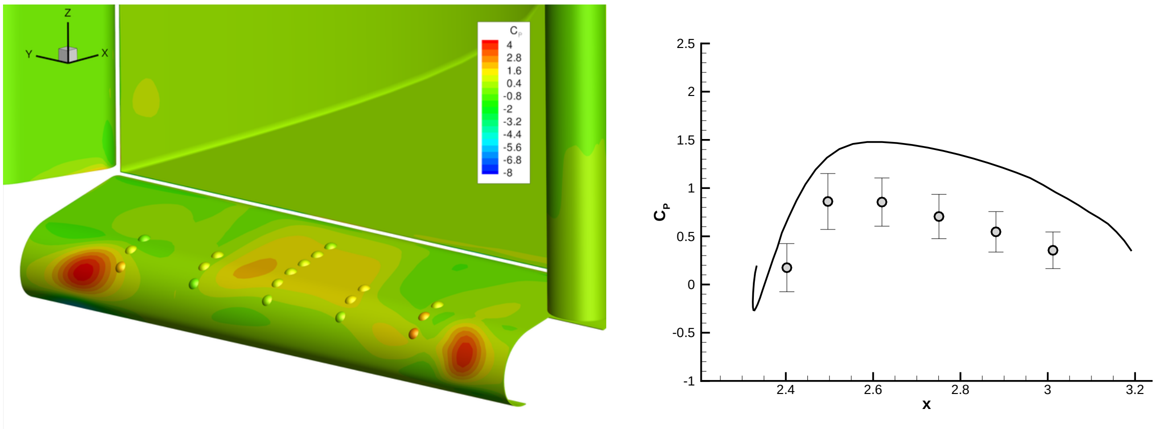

(a) lower deflector (b) symmetry plane

Fig. 22 Pressure coefficient distribution on the lower deflector, $\mu = 0.047$, $C_T/\sigma = 0.12$

At the lower tunnel velocity, $\mu = 0.047$, the rotor wake partly (at $C_T/\sigma = 0.08$) or fully (at $C_T/\sigma = 0.12$) escapes the return circuit. The computed pressure distribution indicates a strong interaction at both thrust values considered (figures 21 and 22), by the presence of high pressure spots on the side portions of the deflector itself. This is partially confirmed by the experimental measurements, which also feature at the side rows pressure sensors a value of the standard deviation larger than 100 %

of the local averaged C_P value. Clearly, in this highly unsteady conditions the comparison of average values becomes meaningless. For the same conditions at $\mu = 0.047$, however, δ at the centerline presents almost uniform values close to 0.18 (19 %) for $C_T/\sigma = 0.08$ and 0.24 (29 %) for $C_T/\sigma = 0.12$, so that the comparisons in figures 21(b) and 22(b) may be considered acceptable.

Overall, the presented comparison exercise, limited to the open test section, shows that the simple steady AD model, utilized in the present calculations, is capable, at least in a qualitative way, to represent the essential features of the rotor flow field and the interaction between rotor wake and tunnel walls. The measurement of the pressure values on the tunnel lower deflector, and in particular of the standard deviation of the unsteady signal, may represent a practical way of monitoring the interference effects.

Conclusions

This work reports the qualitative analysis of the flow inside the closed and open test sections of PoliMi large wind tunnel in the presence of rotor effects. The flow has been simulated with the flow solver *ROSITA*, adopting an actuator disk model of the AW139 rotor to account for the rotor effects in the numerical solution. The load distributions for the development of the actuator disk model were extracted from time-accurate forward flight simulations in free air.

The CFD solutions have been analyzed in order to define the operating parameter range, in terms of wind tunnel speed and rotor thrust, in correspondence of which the flow is qualitatively similar to that of the free air conditions, so that the measured rotor performance can be corrected to account for the wall interference.

In the closed section, the boundaries of the region of these allowed operating parameters corresponds to the occurrence of the flow breakdown, which happens when the interaction between the rotor wake and the wind tunnel walls generates recirculation of the flow in proximity of the rotor. In the PoliMi wind tunnel closed test section, flow breakdown may be avoided, for a rotor load range with $C_T/\sigma \leq 0.12$, selecting advance ratio values larger than 0.07. Moreover, some indications have been given on how to detect on-line the occurrence of flow breakdown during the actual wind tunnel tests by monitoring easily measurable quantities.

The computed flow fields in the open test section appeared to be qualitatively similar to the flow field of the rotor in free-flight conditions for all the operating conditions of interest. Nonetheless, quantitative effects on the measured performance are to be expected, due to the downwash induced by the deviation of the tunnel jet, and the interaction of the rotor wake with the wind tunnel walls, especially for an intermediate range of flow speeds and rotor thrusts where the wake impinges on the lower deflector. In addition, a possibly adverse effect on the performance measurements, due to an unsteady interaction between the wake and the wind tunnel walls, has been described and the operating parameters range where the phenomenon could occur have been identified. A practical means to detect these critical conditions during the actual wind tunnel operations has been given, based on pressure measurement at some selected locations. A limited comparison with pressure measurements on the tunnel lower deflector suggests that the employed simplified AD model is capable to represent the essential qualitative features of the rotor flow field and that the analysis of the standard deviation of the measurements themselves may allow to monitor the stronger interference effects between the rotor wake and the tunnel walls.

Further work is planned to achieve quantitative correction procedures. We believe that the zero flap trim configuration, although easy to be achieved during the experimental tests, is not suitable to correct the performance data to full scale. Shaft load trim is considered to be adequate: it requires true trimming capability both in tunnel flow and free-flight flow, and adequate skill during experimental rotor tests. It will be pursued in a future research effort.

Acknowledgements The present work has been carried out within the WITCH project, funded by AWPARC.

The Authors wish to thank Mr. Gabriele Campanardi and Mr. Donato Grassi for providing the pressure measurements of the open section tests. The Authors are also grateful to the Reviewers for their useful comments, which allowed to improve the quality of the paper.

References

[1] Harris, F. D., “Aerodynamic and Dynamic Rotary Wing Model Testing in Wind Tunnels and Other Facilities,” AGARD LS 63 ”Helicopter Aerodynamics and Dynamics”, 1973.

[2]Philippe, J.-J., "Consideration on wind-tunnel testing techniques for rotorcrafts," AGARD Special Course on Aerodynamics of Rotorcraft, 1990.

[3]Langer, H.-J., Peterson, R. L., and Maier, T. H., "An Experimental Evaluation of Wind Tunnel Wall Correction Methods for Helicopter Performance," American Helicopter Society 52^{nd} Annual Forum Proceedings, Washington, DC, June 1996.

[4]Heyson, H. H., "Jet-Boundary Corrections for Lifting Rotors Centered in Rectangular Wind Tunnels," NASA TR R-71, 1960.

[5]Heyson, H. H., "Use of Superposition in Digital Computers to Obtain Wind-Tunnel Interference Factors for Arbitrary Configurations, with Particular Refernce to V/STOL Models," NASA TR R-302, 1969.

[6]Heyson, H. H., "Fortran Programs for Calculating Wind-Tunnel Boundary Interference," NASA TM X-1740, 1969.

[7]Rae, W.H. Jr., "Limits on Minimum-Speed V/STOL Wind-Tunnel Tests," *Journal of Aircraft* , Vol. 4, (3), 1967, pp. 249–254.

[8]Shinoda, P. M., "Wall interaction effects for a full-scale helicopter rotor in the NASA Ames 80-by 120-foot wind tunnel," AGARD CP 535 "Wall Interference, Support Interference and Flow Field Measurements", 1993.

[9]Biava, M., Boniface, J.-C., and Vigevano, L.,"Influence of wind-tunnel walls in helicopter aerodynamics predictions," 31^{st} European Rotorcraft Forum, Firenze, Italy, September 2005.

[10]Biava, M., "RANS computations of rotor/fuselage unsteady interactional aerodynamics," Ph.D. Thesis, Politecnico di Milano, 2007.

[11]Biava, M., and Vigevano, L., "Simulation of a complete helicopter: A CFD approach to the study of interference effects," *Aerospace Science and Technology*, doi:10.1016/j.ast.2011.08.006, in press, 2011.

[12]Roe, P.L., "Approximate Riemann Solvers, Parameter Vectors and Difference Schemes," *Journal of Computational Physics*, Vol. 43, 1981, pp. 357–372.

[13]Venkatakrishnan, V., "On the accuracy of limiters and convergence to steady state solutions," Paper AIAA 93-0880, 31^{st} AIAA Aerospace Sciences Meeting and Exhibit, Reno, Nevada, 1993.

[14]Jameson, A., “Time Dependent Calculations Using Multigrid with Applications to Unsteady Flows past Airfoils and Wings,” Paper AIAA 91-1596, 10^{th} AIAA Computational Fluid Dynamics Conference, Honolulu, HI, 1991.

[15]Chesshire, G., and Henshaw, W. D., “Composite overlapping meshes for the solution of partial differential equations,” *Journal of Computational Physics*, Vol. 90, 1990, pp. 1–64.